Bulletin of the Seismological Society of America, Vol. 87, No. 6, pp. 1662–1666, December 1997

Short Notes

Do Historical Rates of Seismicity in Southern California Require the Occurrence of Earthquake Magnitudes Greater Than Would be Predicted from Fault Length?

by Mark W. Stirling and Steven G. Wesnousky

Abstract The Working Group on California Earthquake Probabilities reported a discrepancy between the historical rates of large earthquakes in southern California and rates predicted from interpretation of geological, geodetic, and historical seismicity data. It was suggested that the discrepancy may be due to the assumption within their analysis that the magnitude of the largest earthquake on a fault is limited by the mapped fault length. Our analysis of the available data does not support the presence of a historical deficit in the rate of seismicity, nor does it require that earthquakes that rupture beyond the lengths of mapped active faults in southern California, or that rupture numerous subparallel faults, are needed to explain the historical distribution of seismicity.

Introduction

The Working Group on California Earthquake Probabilities (WGCEP, 1995) reported that the number of moderate to large earthquakes predicted from interpretation of geological, geodetic, and historical seismicity data exceeds what has been observed historically in southern California. They further speculated that the discrepancy might have occurred because the effect of using fault length to estimate the maximum size of earthquakes on each fault may have limited the maximum-expected event to a magnitude less than might actually occur. The effect of limiting the maximum-size earthquakes in this manner is that a greater number of earthquakes are required to occur on each fault to satisfy the slip budget, which increases the predicted rate of earthquakes in the region relative to the observed rate. If this latter interpretation is correct, it implies that faults may rupture well beyond the mapped length, or that several faults may rupture simultaneously to produce unusually large earthquakes (Jackson, 1996). We examine whether or not available data require that earthquakes larger than would occur from the mapped lengths are required to reconcile predicted rates of seismicity with those observed historically.

Approach

We restrict our analysis to the area shown in Figure 1, the same area studied by the Working Group on California Earthquake Probabilities (WGCEP, 1995). We show in Figure 2 two plots that are constructed to compare the observed rate of earthquakes in southern California to the rates predicted from interpretation of fault length, slip rate, geodetic, and historical seismicity data. The cumulative number of events per year versus magnitude observed historically in the area is shown by the hachured area labeled "historical" in Figure 2. The historical curve is constructed in each plot by combining a catalog of 49 $M \geqq 6$ earthquakes that have occurred since 1850 (WGCEP, 1995) and events of magnitude 3 to 6 recorded by the CIT-USGS network since 1944. The uncertainty bounds on the historical curve (the width of the hachured area) represent two standard deviations of the cumulative number of events per year and are calculated by assuming that the historical seismicity is represented by a Poisson distribution or, more specifically, that the standard deviation at each magnitude increment is equal to the square root of the cumulative number of events $\geqq M$ divided by the 145-yr time span of recording. The long-term seismicity rates are assumed to lie within these uncertainty bounds.

The WGCEP divided southern California into 65 polygons (Figure 1) and designated each as class A, B, or C, based on the "quantity of available geologic data" for faults in each polygon. The source of seismicity in polygons described as class A and B was taken to be the combination of characteristic earthquakes occurring on major fault zones and a component of distributed seismicity described by the Gutenberg–Richter relationship. Within polygons of class C, seismicity was assumed to satisfy the Gutenberg–Richter distribution, and characteristic earthquakes were assumed to be absent. Toward examining the uncertainties in the estimates in the synthetic rates of seismicity computed by the

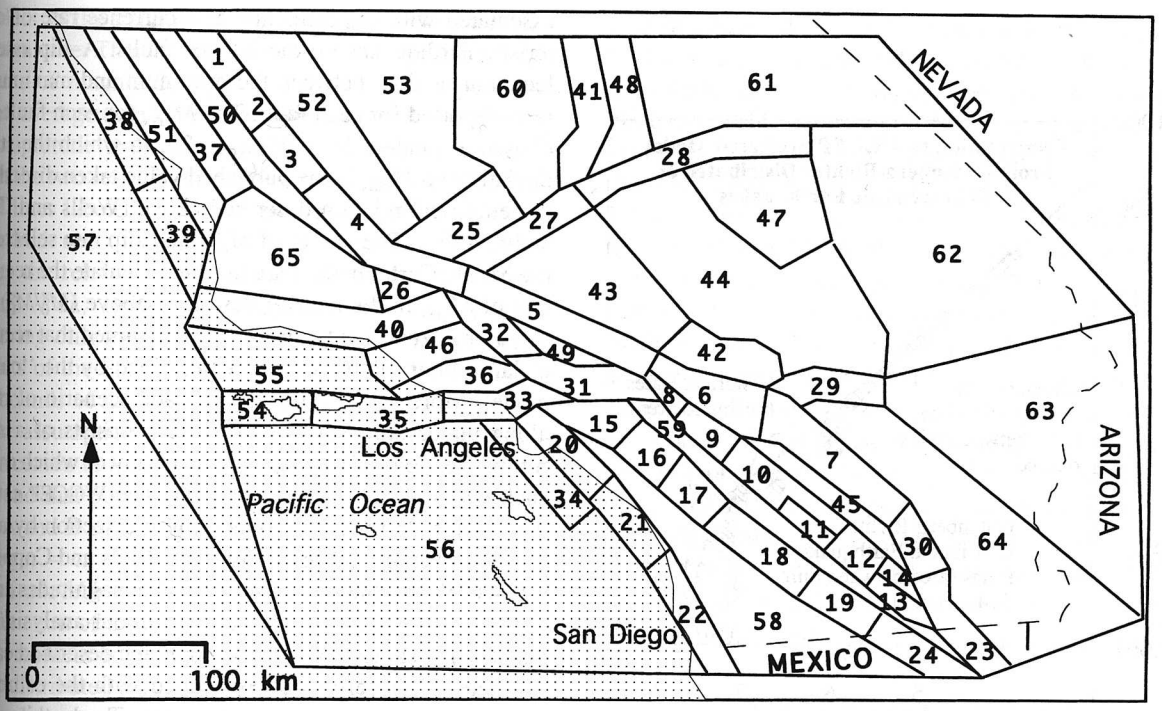

Figure 1. The 65 polygons used by the WGCEP (1995) to define earthquake recurrence rates and sizes in southern California. The WGCEP have classified the polygons A, B, or C according to the quantity of available geologic data for the faults inside each polygon, and the class and name of each is as follows: Class A Polygons: (1) San Andreas-creeping, (2) San Andreas-Parkfield, (3) San Andreas-Cholame, (4) San Andreas-Carrizo, (5) San Andreas-Mojave, (6) San Andreas-San Bernardino, (7) San Andreas-Coachella, (8) San Jacinto-San Bernardino, (9) San Jacinto-San Jacinto, (10) San Jacinto-Anza, (11) San Jacinto-Coyote Ck, (12) San Jacinto-Borrego, (13) San Jacinto-Superstition Mtn, (14) San Jacinto-Superstition Hill, (15) Whittier-Elsinore-Whittier, (16) Whittier-Elsinore-Glen Ivy, (17) Whittier-Elsinore-Temecula, (18) Whittier-Elsinore-Julian, (19) Whittier-Elsinore-Coyote Mtn. Class B Polygons: (20) Newport Inglewood-Onshore, (22) Newport Inglewood-Offshore, (23) Imperial, (24) Laguna-Salada, (25) White Wolf, (26) Big Pine, (27) Garlock-West, (28) Garlock-East, (29) Pinto Mtn, (30) Brawley, (31) Sierra Madre, (32) San Gabriel, (33) Santa Monica-Malibu, (34) Palos Verdes, (35) Santa Cruz Is, (36) Simi San Fernando, (37) Rinconada, (38) Hosgri-North, (39) Hosgri-South, (40) Hosgri-North, (41) Sierra Nevada. Class C Polygons: (42) San Bernardino Mtns, (43) Mojave-West, (44) Mojave-Cent, (45) Salton, (46) Ventura, (47) Mojave-Northeast, (48) Coso, (49) San Gabriel Mtns, (50) Coast Ranges-Cent, (51) Central California Coast, (52) San Joaquin Valley-West, (53) San Joaquin Valley-Cent, (54) Santa Rosa Is, (55) Santa Barbara Channel, (56) Offshore Island, (57) Offshore Cent, (58) Peninsula Ranges-West, (59) Peninsula Ranges-Cent, (60) Southern Sierra Nevada, (61) Basin and Range, (62) Mojave-East, (63) Colorado Corridor, (64) Southeast Corner, (65) Transverse Ranges-West.

WGCEP for all class A, B, and C zones, we examine separately and in the following order the contributions of seismicity arising from (1) rupture of major faults (characteristic earthquakes) and (2) that seismicity assumed to be distributed within the polygons and characterized by a magnitude-frequency distribution described by the Gutenberg–Richter relationship.

We initially describe the approach used to define the recurrence rates of characteristic earthquakes on the B zone faults and follow that with a description of the treatment of the largest earthquakes on the A zone faults. For the B zone faults, a characteristic earthquake size (M_{max}) was defined by the WGCEP from the length of the mapped fault traces in each class B polygon and by application of an empirical relationship that relates the magnitude of an earthquake to the fault rupture length (Wells and Coppersmith, 1994). We calculate the characteristic earthquake rates for the B zone faults by converting the M_{max} for each zone to seismic moment M_0^e with the relationship Log $M_0^e = 1.5M + 16.1$ (Hanks and Kanamori, 1979). The recurrence rate of M_{max} earthquakes is taken to equal $\dot{M}_0^g/M_0^e$, where $\dot{M}_0^g$ is proportional to fault slip rate and equals the average rate of seismic moment release on the fault (e.g., Wesnousky, 1994). We use a Monte Carlo approach to estimate the uncertainties

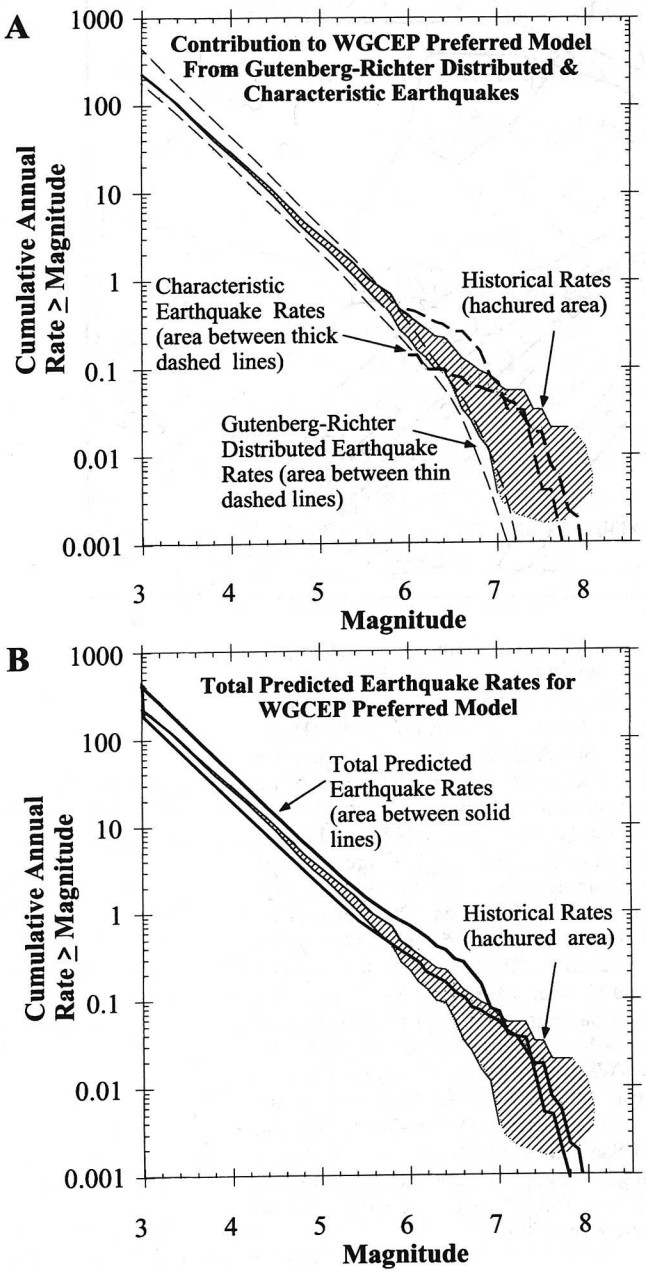

Figure 2. Plots of the cumulative number of events per year greater than or equal to a given magnitude observed historically in southern California (hachured area) and rates predicted from the Preferred Model of the WGCEP (1995). Plot (a) shows the contribution to the total predicted rate from Gutenberg–Richter distributed earthquakes (thin dashed lines) and characteristic earthquakes (thick dashed lines). Plot (b) shows the total predicted rate (solid lines). The historical distributions show uncertainty bounds that represent two standard deviations of the mean rates.

associated with the estimates of recurrence rate of characteristic earthquakes on the B zone faults. A slip rate is selected at random between the minimum and maximum slip rates reported for each fault. The M_{max} for each fault is then chosen at random from $M_{max} \pm 2\sigma$, in which the standard deviation on M_{max} is the published value taken directly from the empirical relation described above (Wells and Coppersmith, 1994). The values of M_{max} and slip rate selected with the Monte Carlo method are used to calculate the recurrence rate of M_{max} in the manner described above ($\dot{M}_0^g/M_0^e$).

For A zone faults, the WGCEP assumed that recurrence of large fault rupture events is described by the "cascade" model. More specifically, the cascade scenario of ruptures along major faults in class A zones consists of a suite of rupture sections of varying lengths (many of which overlap), each with specific recurrence rates. The WGCEP estimated the magnitude for each cascade rupture section by application of the empirical relationship of Wells and Coppersmith (1994). We use the cascade earthquake magnitudes and rates of the WGCEP (1995, their Table 3) in our analysis, but we also use the same Monte Carlo approach described earlier to estimate the uncertainties associated with the estimates of recurrence rates of these earthquakes. To do this, we first calculate the contribution of slip rate ($\dot{U}'$) to the total slip rate ($\dot{U}$) that is accounted for by the repeated rupture of each cascade rupture section. In this manner, the slip rate $\dot{U}'$ is taken to equal $\dot{M}_0^g/\mu LW$, in which $\dot{M}_0^g$ is the seismic moment release rate (equal to the recurrence rate of the cascade rupture $\times\ 10^{(1.5Mw\ +\ 16.1)}$; Mw = the cascade magnitude), μ is the rigidity modulus (3×10^{11} dyne/cm^2), and L and W are the length and width (15 km) of each cascade rupture section. Minimum and maximum bounds on the contribution ($\dot{U}'$) to total fault slip rate represented by the repeated rupture of each cascade rupture section are assumed to be proportional to the uncertainty reported for the fault slip rate ($\dot{U}$). Thus, if the fault slip rate is $\dot{U} \pm 0.1\dot{U}$ cm/yr, then the uncertainty in the slip rate $\dot{U}'$ contributed by a particular cascade type of event is taken to equal $\dot{U}' \pm 0.1\dot{U}'$ cm/yr. With the slip rates and uncertainties so defined, we then use the same methods described above for the B zones to select a slip rate and magnitude at random from the minimum and maximum bounds of each cascade slip rate and magnitude, and to calculate the recurrence rates of the magnitude for each cascade rupture section.

Five hundred cycles are made through all of the A zone cascade ruptures and B zone faults in the manner described earlier before the mean of the cumulative number of events per year ≧M, and the uncertainty bounds ($\pm 2\sigma$) are computed for the entire data set. The mean and standard deviation do not change when more than 500 cycles are made. To be sure that we do not consistently underestimate the M_{max} of each B zone fault, or the magnitude of each cascade rupture section, we also undertake a second set of simulations that differ from the first set in the way that the magnitude is calculated. For these simulations, a seismic moment is chosen at random from the range of seismic moments that are

equivalent to the magnitude $\pm 2\sigma$ and then converted back to a magnitude. This latter approach works to produce larger estimates of magnitude and, as a result, lower recurrence rates on average than when the magnitude is chosen directly from magnitude $\pm 2\sigma$. The range of recurrence rates calculated in the two sets of simulations is shown by the two thick dashed lines labeled "characteristic earthquake" on Figure 2a. For both sets of simulations, we ensure that every cycle satisfies the relative plate motion rate of 48 ± 2 mm/yr (DeMets *et al.,* 1990; Humphreys and Weldon, 1994) by considering only cycles for which the total slip rate across the faults of the San Andreas system are within the uncertainty bounds of the plate motion rate.

The assumption used in calculation of the Gutenberg–Richter curves in Figure 2a is that all of the seismicity in C zones, and that portion of seismicity not occurring directly on the A and B zone faults, is characterized by the relationship $\text{Log } n = a - bM$, in which n is the number of events of magnitude M, b is assumed to equal 1, and the productivity a is a function of the size of M_{max} and the proportion of the seismic moment release assumed to occur by Gutenberg–Richter distributed earthquakes (WGCEP, 1995). For each of the 65 polygons, we use the estimates of M_{max} together with the seismic moment release rates for distributed earthquakes in each polygon (WGCEP, 1995, their Table 5) and equations of Anderson and Luco (1983) to calculate the number of events per year for each increment of magnitude. These rates are then combined to calculate the cumulative number of events per year greater than or equal to a given magnitude (N/yr) for the region (Fig. 2a). We repeat these calculations three times using equations I.5, II.5, and III.5 of Anderson and Luco (1983), respectively. The three equations produce recurrence rates that differ by about a factor of 2 at small to moderate magnitudes because of the way that each equation truncates the recurrence rates of M_{max}. The area enclosed by the thin dashed lines in Figure 2a shows the range of recurrence rates calculated from the three equations for that portion of seismicity distributed according to the Gutenberg–Richter relationship.

The curves labeled "total predicted" in Figure 2b are the sum of the extreme values of the curves labeled "Gutenberg–Richter" and "characteristic earthquake" in Figure 2a. The uncertainty bounds on the predicted seismicity (total predicted, solid lines) overlaps substantially with the uncertainty bounds on the historical seismicity (hachured area) from small to large magnitudes, except at M 6 to 7 where the overlap is less pronounced. It thus appears difficult to argue that any differences between the historical and predicted rates are significant.

We may also take another approach to test the statistical significance of the WGCEP discrepancy. In this approach, we examine the likelihood that a 145-yr "sample" from the predicted rates would yield the rate of seismicity observed in the last 145 years. We initially convert the total predicted curves in Figure 2b to the equivalent minimum and maximum incremental recurrence rates (number of events per year of magnitude M) and then use a Monte Carlo method to choose a rate at random between these extremes for each magnitude interval. The rate is then multiplied by the sampling time (145 years) to give the expected number of events (n) of magnitude M for that time period. Finally, we assume that each n is described by a Poisson distribution and choose a final value at random from a Poisson distribution with mean equal to n. The final value of n is then converted back to the number of events per year. In Figure 3, we show the number of events per year versus magnitude observed in southern California (solid circles) and the number of events per year produced from 500 repetitions of the above procedure (dots). The numbers shown on the graph at $M \geqq 6$ (Fig. 3) represent the percentages of simulations that yield rates less than or equal to the rates observed historically. These percentages do not change for a greater number of repetitions. In this case, we observe that the historical seismicity rates fall well within the rates calculated from the total predicted curves for the same period of time and for the entire range of magnitudes.

Discussion and Conclusions

We have used essentially the same data and a procedure similar to the WGCEP (1995) to calculate the total earthquake rate for the region, with an aim toward placing uncertainty

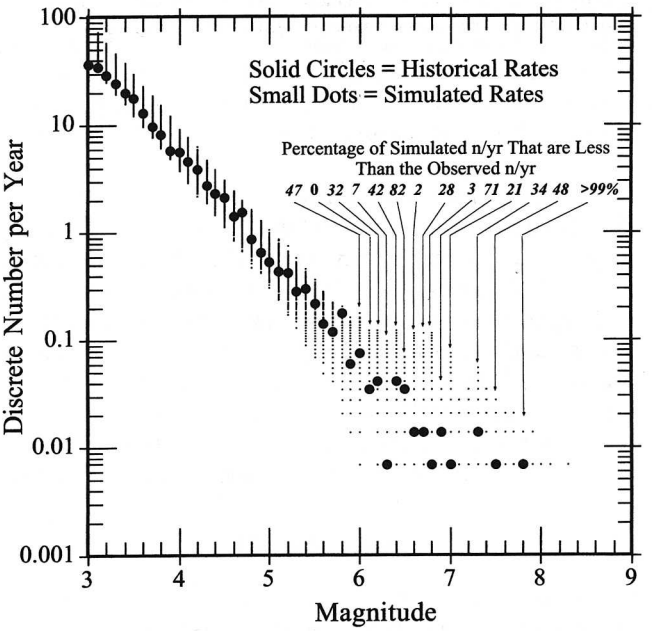

Figure 3. Plot of the discrete number of events per year versus magnitude observed historically in southern California (solid circles), and predicted from 500 random catalogs drawn from the total predicted curves in Figure 2b (dots). Note that many of the dots displayed on the figure represent more than one simulation and that the dots merge to form vertical lines at magnitudes less than about 5.5. Also note that many simulations produce 0 earthquakes at $M \geqq 6.2$.

bounds on size and rate distribution of earthquakes expected from interpretation of geologic, geodetic, and historical seismicity data. Using either of two approaches, we find that the historical recurrence rates generally lie well within the range of predicted recurrence rates (Figs. 2b and 3). In addition to the uncertainties we have included in this analysis, there also exist other uncertainties that have not been considered, such as those attributed to temporal fluctuations in the Gutenberg–Richter distributed recurrence rates and uncertainties in the recurrence rates that arise from the use of different empirical regressions to estimate earthquake magnitude (e.g., Wells and Coppersmith, 1994; Anderson *et al.,* 1996). Consideration of any further uncertainties would be expected to increase the overlap between the predicted and historical rates in Figures 2b and 3. Thus, our analysis of the data currently available does not support the presence of a historical deficit in the rate of seismicity, nor does it require that unusually large earthquakes that rupture beyond the lengths of mapped active faults in southern California, or that rupture numerous subparallel faults, are needed to explain the historical distribution of seismicity.

Acknowledgments

We thank Dave Jackson for his review of the manuscript and guidance in aspects of the analysis, and John Anderson, Jim Brune, Glenn Biasi, and Sergio Chavez-Perez for their comments on an earlier draft. The work was funded by the Southern California Earthquake Center (Publication Number 340). Center for Neotectonic Studies Contribution Number 21.

References

Anderson, J. G. and J. E. Luco (1983). Consequences of slip rate constraints on the earthquake occurrence relation, *Bull. Seism. Soc. Am.* **73,** 471–496.

Anderson, J. G., S. G. Wesnousky, and M. W. Stirling (1996). Earthquake size as a function of fault slip rate, *Bull. Seism. Soc. Am.* **86,** 683–690.

DeMets, C., R. G. Gordon, D. F. Argus, and S. Stein (1990). Current plate motions, *Geophys. J. Int.* **101,** 425–478.

Hanks, T. C. and H. Kanâmori (1979). A moment magnitude scale, *J. Geophys. Res.* **84,** 2348–2350.

Humphreys, E. D. and R. J. Weldon (1994). Deformation across the western United States: a local estimate of Pacific-North American transform deformation, *J. Geophys. Res.* **99,** 19975–20010.

Jackson, D. D. (1996). The case for huge earthquakes, *Seism. Res. Lett.* **67** (1), 3–5.

Petersen, M. D. and S. G. Wesnousky (1994). Fault slip rates and earthquake histories for active faults in southern California, *Bull. Seism. Soc. Am.* **84,** 1608–1649.

Wells, D. L. and K. J. Coppersmith (1994). New empirical relationships among magnitude, rupture length, rupture width, rupture area, and surface displacement, *Bull. Seism. Soc. Am.* **84,** 974–1002.

Wesnousky, S. G. (1994). The Gutenberg-Richter or characteristic earthquake distribution, which is it?, *Bull. Seism. Soc. Am.* **84,** 1940–1959.

Working Group on California Earthquake Probabilities (1995). Seismic hazards in southern California: probable earthquakes, 1994–2024, *Bull. Seism. Soc. Am.* **85,** 379–439.

Center for Neotectonic Studies and Department of Geological Sciences
University of Nevada
Reno, Nevada 89557

Manuscript received 15 July 1996.